Integrating dissipative particle dynamics with energy conservation

Isamu Kusaka* and Nicholas T. Liesen
William G. Lowrie Department of Chemical and Biomolecular Engineering, 512 Koffolt Laboratories, Ohio State University, CBEC, 151 West Woodruff Avenue, Columbus, Ohio 43210-1350, USA

(Received 1 October 2019; revised manuscript received 21 February 2020; accepted 19 March 2020; published 17 April 2020)

To suppress secular energy drift in dissipative particle dynamics simulations with energy conservation, we introduce an additional pairwise particle dynamics that allows for a microscopic energy fluctuation while conserving the total linear momentum of the system exactly. The pairwise dynamics may be regarded as an adaptation of the thermostat in isothermal dissipative particle dynamics, but leads to microcanonical instead of canonical ensemble at equilibrium and allows for a nonuniform temperature field at a steady state. The method is also effective in suppressing secular energy drift when used in combination with reverse nonequilibrium molecular dynamics moves. All of the equilibrium and transport properties we computed were unaffected by this additional pairwise dynamics.

DOI: 10.1103/PhysRevE.101.042120

I. INTRODUCTION

The velocity Verlet algorithm (VV) [1,2] plays an integral part in molecular dynamics simulation (MD) and is often used within a more general particle-based simulation such as dissipative particle dynamics (DPD) [3]. In the Shardlow splitting algorithm (SSA) [4], for example, the equations of motion of DPD are split into conservative dynamics on the one hand and dissipative and fluctuating dynamics on the other. The first part of dynamics is usually integrated by VV, while integration of the latter relies on the existing integration methods for Langevin equations [5,6].

VV has many desirable properties: It preserves the fundamental properties of the equations of motion of classical mechanics, such as microscopic reversibility and phase volume invariance. In addition, it conserves the so-called shadow Hamiltonian [7–9] extremely well. The difference between the shadow Hamiltonian and the actual Hamiltonian can be expressed as a power series in Δt, the time step of integration, with the leading term proportional to $(\Delta t)^2$ [10]. Thus, provided that Δt is smaller than the (generally unknown) radius of convergence of the series, VV produces a trajectory of nearly constant energy over an extremely long duration of time.

Nevertheless, VV gives rise to a energy drift if it is used *in combination with* additional dynamics that conserve energy exactly. That is, the total energy of the system, on average, changes monotonically with time and is no longer bounded. As pointed out in Refs. [11,12], this is indeed the case with SSA applied to DPD with energy conservation (DPDE) [13,14]. Reverse nonequilibrium molecular dynamics (RNEMD) [15], which aims to extract transport properties of a system by imposing a flux and measuring the resulting steady-state response, is another example. To avoid energy drift, calculation of viscosity using RNEMD is often carried out in isothermal ensembles, while more elaborate integration schemes must be adopted for thermal conductivity computation [16,17].

The energy drift observed in these simulations can be understood as follows [11,12]. The dissipative and fluctuating dynamics in DPDE and the swap moves in RNEMD conserve the energy exactly. In contrast, the quantity (extremely well) conserved in VV is the shadow Hamiltonian and not the energy. Thus, VV moves the system along a constant shadow Hamiltonian path on which the energy is not constant. The subsequent dissipative and fluctuating dynamics (or the swap moves in RNEMD) carries the system along a constant energy path, thus affecting the value of the shadow Hamiltonian. Repeated applications of these two dynamics, in general, would not conserve either of these quantities. It does not appear reasonable to expect that the fluctuations of these quantities are somehow bounded along the phase trajectory thus generated. In short, it is a combination of small (and bounded) energy fluctuations of VV and exact energy conservation of DPDE or RNEMD that produces unbounded energy drift.

This observation suggests that one may eliminate the secular energy drift either by altering the dissipative and fluctuating dynamics of DPDE (or the swap move in RNEMD) so that the shadow Hamiltonian is conserved or by using an energy-conserving algorithm for the conservative dynamics. However, the explicit form of the shadow Hamiltonian is unknown except for simple model systems such as a single harmonic oscillator. On the other hand, application of strictly energy-conserving integrators [18–20] to a system with a large number of mechanical degrees of freedom is a nontrivial computational task.

A nonsmooth interparticle potential is another source of the energy drift [21,22]. The shadow Hamiltonian exhibits a jump when the system crosses the point of discontinuity in interparticle potential or its derivatives. This is the case when the potential function is truncated (by necessity when

*kusaka.2@osu.edu

 ©2020 American Physical Society

using periodic boundary conditions) unless it is augmented by a carefully constructed switching function. The issue is expected to be particularly acute for DPD, in which the most commonly used potential function has the discontinuous second derivative and a typical particle number density is in the range of 3 to 10.

In all cases mentioned above, the energy drift can be reduced by using a smaller time step for integration. However, it cannot be eliminated completely in this manner and in principle, if not in practice, precludes steady or equilibrium states from our consideration. This restriction on the time step severely limits our ability to simulate a long time behavior of a system and runs counter to the very aim of DPD(E), which is to access mesoscopic timescales. In fact, a considerable effort has been made since the inception of DPD to eliminate time-step dependence of various equilibrium and transport properties, thus allowing for a larger time step to be used [23–28].

Thus far, such an effort has been directed toward the isothermal DPD. In this case, the built-in thermostat that maintains the system at a given temperature also prevents a systematic energy drift. In contrast, however, DPDE aims to simulate an isolated system and the demand of energy conservation places a far stricter limit on the admissible size of Δt.

Given the widespread use of nonsmooth interaction potentials in DPD(E) as well as the ease at which RNEMD (with or without the dissipative and fluctuating dynamics of DPDE) can drive nonequilibrium processes in general (even beyond what is usually considered in computation of transport properties and including a simulation of thermocapillary flows, for example), it seems desirable to have a simple method to eliminate the secular energy drift in these simulations.

Energy conservation can be enforced exactly by means of a projection method, in which either the velocities or the internal energies of the individual particles are adjusted [11,12]. The former method affects the total linear momentum of the system and hence would not be appropriate for studying phenomena involving convective fluxes. The latter method is free from this shortcoming but applies only to DPDE.

In search for a method that conserves linear momentum and at the same time is uniformly applicable whether or not the particles have internal degrees of freedom, we recall that macroscopic systems, whose behavior we wish to understand by means of MD simulation, are never truly isolated from their surroundings, and even the slightest of interactions with the surroundings (in a form of an experimental measurement, for example) causes the system energy to fluctuate. Thus, isolated systems of our interest are generally associated with a very small but still nonzero energy fluctuations, whose magnitude we shall denote by ΔE. In fact, we recall that such ΔE is essential in the definition of the entropy of an isolated system in statistical mechanics and that the exact value of ΔE has no quantitative consequence for intensive quantities of the system in equilibrium [29–31]. (Strictly speaking, ΔE in statistical mechanics is usually attributed to the uncertainty principle and its magnitude is much smaller than those associated with numerical integration of the equations of motion. Insofar as the intensive quantities are insensitive to the magnitude of ΔE, this observation is not relevant to what follows.) Because interaction of a similar magnitude should exist between a system and its surroundings regardless of what else may be happening in the system, a nonzero ΔE should be admissible when simulating time-dependent processes as well.

In simulations of many-particle systems, therefore, the importance should be placed not on the exact energy conservation but on ensuring that the energy fluctuations are reasonably small and that the system energy is bounded. By discarding the hard constraint in favor of a less stringent one, we may gain some flexibility in designing an integration scheme. Indeed, VV is such a method, but only for sufficiently smooth interparticle potentials in the absence of an additional dynamics that conserves energy exactly.

Motivated by the momentum-conserving Lowe-Andersen thermostat [23,32], we introduce an additional pairwise dynamics that allows for small fluctuations in energy while ensuring strict conservation of the total linear momentum. This method, which we will call energy dissipation dynamics (EDD), completely eliminates the secular energy drift both in DPDE and in RNEMD without affecting any of the equilibrium or transport properties we examined.

We will briefly summarize equations of motion of DPD(E) and the basic ideas of RNEMD method in Sec. II. In Sec. III, we introduce EDD and show that its equilibrium distribution is microcanonical. The integration scheme incorporating EDD is expressed in terms of the propagator of dynamics in Sec. IV. Section V describes the application of EDD to typical model systems in DPD. The results from simulations are given in Sec. VI. The article concludes with a brief summary in Sec. VII. The integration scheme for the dissipative and fluctuating dynamics of DPDE is described in detail in Appendix A. Appendix B compares our integration method for viscous heating dynamics (a subdynamics of DPDE) with the corresponding algorithm in Ref. [11], which extends the work of Shardlow [4] for DPDE. Appendix C is concerned with an aspect unique to the thermal conductivity calculation when RENMD is used with DPDE.

II. EQUATIONS OF MOTION

Molecular dynamics simulation solves a set of Newton's equations of motion for a system of N particles:

$$d\mathbf{r}_i = \mathbf{v}_i dt \quad \text{and} \quad d\mathbf{v}_i = \sum_{j\neq i} \frac{\mathbf{F}^c_{ij}}{m_i} dt, \tag{1}$$

where i runs from 1 through N, the sum is with respect to j running from 1 through N excluding i, and m_i, $\mathbf{r}_i$, and $\mathbf{v}_i$ are, mass, position, and velocity of particle i, respectively. $\mathbf{F}^c_{ij}$ is a conservative force exerted onto particle i by particle j.

In DPDE, the conservative dynamics is supplemented by dissipative and fluctuating dynamics in such a way as to conserve the total energy of the system:

$$d\mathbf{r}_i = \mathbf{v}_i dt, \tag{2a}$$

$$d\mathbf{v}_i = \sum_{j\neq i} \left[\frac{\mathbf{F}^c_{ij}}{m_i} dt - \frac{\gamma_{ij}}{m_i} {\omega_{ij}}^2 v^e_{ij} \mathbf{e}_{ij} dt + \frac{\sigma}{m_i} \omega_{ij} \mathbf{e}_{ij} \circ dW^v_{ij} \right], \tag{2b}$$

$$d\epsilon_i = \sum_{j\neq i} \frac{1}{2}\left[\gamma_{ij} {v_{ij}^e}^2 + \alpha^2\left(\frac{c_i}{\epsilon_i} - \frac{c_j}{\epsilon_j}\right)\right]{\omega_{ij}}^2 dt + \sum_{j\neq i}\left[-\frac{1}{2}\sigma\omega_{ij} v_{ij}^e \circ dW_{ij}^v + \alpha\omega_{ij}\circ dW_{ij}^\epsilon\right]. \tag{2c}$$

where $\mathbf{e}_{ij} := (\mathbf{r}_i - \mathbf{r}_j)/r_{ij}$, in which $r_{ij} := \|\mathbf{r}_i - \mathbf{r}_j\|$, is a unit vector pointing from particle j to particle i, and $v_{ij}^e := (\mathbf{v}_i - \mathbf{v}_j)\cdot\mathbf{e}_{ij}$. The weighting function $\omega_{ij} = \omega_{ji}$ specifies the range of the dissipative and fluctuating forces between the particles. Furthermore, c_i is the heat capacity and ϵ_i is the internal energy, both referring to particle i. The constants γ_{ij} and σ control the strength of dissipative and random forces between particles i and j. According to the fluctuation-dissipation theorem, the equilibrium distribution of DPDE is microcanonical if [13,14]

$$\gamma_{ij} = \frac{\sigma^2}{4}\left(\frac{c_i}{\epsilon_i} + \frac{c_j}{\epsilon_j}\right). \tag{3}$$

Likewise, α controls the heat conduction dynamics among the particles. The infinitesimal quantities $dW_{ij}^v = dW_{ji}^v$ and $dW_{ij}^\epsilon = -dW_{ji}^\epsilon$ denote increments of Wiener processes. As denoted by the symbol $\circ$, the stochastic differential equations are to be understood according to the Stratonovich interpretation [33].

If the equations of motion for ϵ_i are omitted, the total energy of the system is no longer conserved. Additionally, if Eq. (3) is replaced by

$$\gamma_{ij} = \frac{\sigma^2}{2k_BT}, \tag{4}$$

where k_B is the Boltzmann constant and T is the absolute temperature, the equations of motion for DPDE reduce to those of DPD and give rise to the canonical distribution at equilibrium.

In order to integrate the equations of motion of DPD(E) numerically, one splits the equations into two subdynamics, one pertaining to the conservative dynamics only and the other to dissipative and fluctuating dynamics. Since each subdynamics conserves the total energy of the system, this Shardlow splitting algorithm (SSA) [4] leaves the equilibrium distribution (a function only of the total energy) unaffected. This accounts for the success of SSA.

When the conservative dynamics is further divided in VV, the energy is no longer conserved exactly. This does not introduce any practical difficulty *provided that* VV is used in isolation as in MD in microcanonical ensemble or in combination with an appropriate thermostat such as the Nosé-Hoover thermostat or as in DPD.

In addition to the dynamics we have discussed so far, RNEMD for shear viscosity calculation introduces a swap move, in which one of the components of the velocity vector is swapped between suitably chosen pair of particles. In RNEMD, therefore, the velocity gradient is generated by "Maxwell's demon" rather than by an externally imposed force as in standard nonequilibrium simulations. This would make any attempt to write equations of motion for RNEMD moves a contrived one. In what follows, it is sufficient to note that RNEMD moves conserve both the total linear momentum and the total energy of the system exactly. A similar remark applies to RNEMD for thermal conductivity calculation, in which all components of the velocity vectors are swapped between a suitably chosen pair of particles.

For brevity, we shall refer to the entirety of the conservative dynamics, dissipative, and fluctuating dynamics of DPD(E), and RNEMD moves as the primary dynamics.

Our integration scheme employs SSA and its details are presented in Sec. IV and Appendix A. Here, it is sufficient to note that the dissipative and fluctuating dynamics of DPDE is decomposed down to the level of a single pair of interacting particles. In what follows, therefore, we will write equations of motion only for one such pair.

III. THEORY

As discussed already, the unbounded energy drift is a numerical issue of the integration scheme for the primary dynamics and arises from small energy fluctuations in VV combined with constant energy moves of DPDE or RNEMD. Nevertheless, it is useful to consider the energy fluctuations and drift as originating from an interaction between the system and its surroundings. This is an acceptable viewpoint provided that these two causes of energy fluctuations and drift cannot be distinguished on the basis of observable behavior of the system in simulation. Without further details regarding the nature of the surroundings, its interaction with the system is best described as a stochastic process.

Thus, we formally regard the primary dynamics as consisting of (1) the exact dynamics, a part that conserves the energy and the total linear momentum exactly and (2) a stochastic process. In this way, the stochastic process is entirely responsible for the unbounded energy drift. To control this, we introduce an additional dissipative mechanism, referred to as the energy dissipation dynamics (EDD), which results in the velocity updating scheme given by Eq. (13) below.

Since both primary and exact dynamics conserve the total linear momentum of the system exactly, the same is true for the stochastic process. Demanding the same of the dissipative dynamics, we put forward the following equations of motion, written for each pair of particles i and j in the system, to describe the dissipative and stochastic processes:

$$\begin{aligned} m_i d\mathbf{v}_i &= -g_{ij} v_{ij}^e \mathbf{e}_{ij} dt + \mathbf{e}_{ij} dX_{ij} \\ m_j d\mathbf{v}_j &= g_{ij} v_{ij}^e \mathbf{e}_{ij} dt - \mathbf{e}_{ij} dX_{ij}, \end{aligned} \tag{5}$$

where dX_{ij} is the stochastic process we are considering and g_{ij} characterizes the dissipative force of EDD.

In writing Eq. (5), we have tacitly assumed that the interaction with the surroundings affects velocities of particles but not their positions. A justification for this simplifying assumption can be given only on the basis of the usefulness of the resulting approach.

Our goal now is to construct an appropriate dissipative process g_{ij} so that the total energy of the system remains bounded. For this purpose, we must first understand how the system energy behaves under Eq. (5).

The pairwise dynamics conserves the linear momentum of the pair exactly since $m_i d\mathbf{v}_i + m_j d\mathbf{v}_j = \mathbf{0}$. However, the kinetic energy $K_i + K_j$ of the particles i and j will be affected

by the indicated changes in $\mathbf{v}_i$ and $\mathbf{v}_j$:

$$d(K_i + K_j) = -g_{ij}\left(v_{ij}^e\right)^2 dt + v_{ij}^e dX_{ij} + dY_{ij}, \tag{6}$$

where $dY_{ij} := (m_i\|d\mathbf{v}_i\|^2 + m_j\|d\mathbf{v}_j\|^2)/2$. Since the potential energy due to the interaction between particles i and j is unaffected by the changes in their velocities, Eq. (6) summed over all pairs of particles in the system may be written as

$$d(K + U - E_0) = -\sum_{(i,j)} g_{ij}\left(v_{ij}^e\right)^2 dt + NdZ, \tag{7}$$

where K and U are, respectively, total kinetic and potential energies of the system, N is the total number of particles, and E_0 is a constant. The sum of the stochastic processes $NdZ := \sum_{(i,j)}(v_{ij}^e dX_{ij} + dY_{ij})$ is itself a stochastic process and represents the energy drift and fluctuations arising from the integrator of the primary dynamics. On an empirical basis, it appears reasonable to expect that dZ can be expressed as the sum of a secular drift term Adt and a stochastic term BdW, where A and B are constant and dW is an increment of the Wiener process. This gives the stochastic differential equation

$$df = \left[A - \frac{1}{N}\sum_{(i,j)} g_{ij}\left(v_{ij}^e\right)^2\right]dt + BdW, \tag{8}$$

where $f := (K + U - E_0)/N$ is the deviation per particle of the system energy from some specified constant E_0. In DPDE, the internal energy of each particle must be included in the total energy of the system. However, because the internal energy remains constant in the pairwise dynamics under consideration, it will not be made explicit in what follows.

Let

$$g_{ij} = \frac{\chi f}{C_2}\mu_{ij}\theta(R_c - r_{ij}), \tag{9}$$

where $\mu_{ij} := m_i m_j/(m_i + m_j)$ is the reduced mass, χ is a constant controlling the strength of the dissipative force, θ is a step function with R_c denoting the cutoff distance [$\theta(x) = 1$ if $x \geqslant 0$ and $\theta(x) = 0$ otherwise], and

$$C_2 := \frac{1}{N}\sum_{(i,j)} \mu_{ij}\theta(R_c - r_{ij})\left(v_{ij}^e\right)^2. \tag{10}$$

For this choice of g_{ij},

$$df = (A - \chi f)dt + BdW \tag{11}$$

and the equilibrium distribution $p(f)$ for f is given by

$$p(f) = \sqrt{\frac{\chi}{\pi B^2}}\exp\left[-\frac{\chi(f - A/\chi)^2}{B^2}\right]. \tag{12}$$

Since the exact dynamics leaves the system energy unaffected, Eq. (12), which was obtained for Eq. (5), is also the equilibrium distribution of the entire simulation consisting of the primary dynamics and the energy dissipation mechanism introduced in this section. For a suitable choice of the constant χ, the distribution will be sufficiently narrow and the energy is practically bounded. If ergodicity is assumed, this means that the corresponding statistical ensemble is essentially microcanonical.

Equations (5) and (9) lead to the following velocity update scheme for each pair of particles:

$$\begin{aligned}\Delta\mathbf{v}_i &= -\frac{\chi f}{C_2}\frac{\mu_{ij}}{m_i}\theta(R_c - r_{ij})v_{ij}^e\mathbf{e}_{ij}\Delta t,\\ \Delta\mathbf{v}_j &= \frac{\chi f}{C_2}\frac{\mu_{ij}}{m_j}\theta(R_c - r_{ij})v_{ij}^e\mathbf{e}_{ij}\Delta t,\end{aligned} \tag{13}$$

where Δt is the time step of integration. The stochastic noise term dX_{ij} in Eq. (5) represents the net effect arising from the integration scheme for the primary dynamics and should *not* be included explicitly in Eq. (13).

IV. INTEGRATION OF THE EQUATIONS OF MOTION

Let $\mathcal{L}$ denote the generator of the dynamics consisting of $\mathcal{L}^C$, $\mathcal{L}^E$, and $\mathcal{L}^D$ representing, respectively, the generators of the conservative dynamics driven by the Hamiltonian, EDD, and the fluctuating and dissipating dynamics of DPDE:

$$\mathcal{L} = \mathcal{L}^C + \mathcal{L}^E + \mathcal{L}^D. \tag{14}$$

Denoting by $\mathcal{R}$ an operator which acts on a microstate to carry out a swap move of RNEMD with a certain probability, which is proportional to Δt, we express the propagator for the most general simulations we considered as $\mathcal{R}e^{\mathcal{L}\Delta t}$. This operator acts on the microstate at time t and produces the corresponding macrostate at $t + \Delta t$.

Invoking SSA, we write

$$\mathcal{R}e^{\mathcal{L}\Delta t} \approx \mathcal{R}e^{\mathcal{L}^D\Delta t}e^{\mathcal{L}^E\Delta t}e^{\mathcal{L}^C\Delta t}. \tag{15}$$

Omission of certain factors on the right-hand side results in a propagator for a less general simulation. For example, $\mathcal{R}$ will be missing in an equilibrium simulation. If the factor $e^{\mathcal{L}^C\Delta t}$ alone is retained, the propagator leads to an equilibrium MD simulation. If $e^{\mathcal{L}^E\Delta t}$ is dropped, the resulting simulation has no energy control measure. This is the case with DPD, which simulates a system in contact with a heat bath. If strict energy conservation is imposed by means of a projection method, $e^{\mathcal{L}^E\Delta t}$ needs to be replaced by an operator $\mathcal{P}_v$ or $\mathcal{P}_i$ representing, respectively, rescaling of particle velocities or of internal energies of individual particles.

The velocity Verlet algorithm is a symplectic method of the second order and is given by

$$e^{\mathcal{L}^C\Delta t} \approx \mathcal{S}_2(\Delta t) := e^{\mathcal{L}^v\Delta t/2}e^{\mathcal{L}^r\Delta t}e^{\mathcal{L}^v\Delta t/2}, \tag{16}$$

where

$$\mathcal{L}^r := \sum_i \mathbf{v}_i\cdot\frac{\partial}{\partial\mathbf{r}_i} \quad\text{and}\quad \mathcal{L}^v := \sum_i \frac{\mathbf{F}_i^C}{m_i}\cdot\frac{\partial}{\partial\mathbf{v}_i}. \tag{17}$$

Here, $\mathbf{F}_i^C$ denotes the total conservative force acting on the particle i and the sum is over all particles in the system. Following Ref. [28], we also consider the effect of using a fourth-order symplectic method [7], which is given by

$$e^{\mathcal{L}^C\Delta t} \approx \mathcal{S}_2(\tau_1)\mathcal{S}_2(\tau_0)\mathcal{S}_2(\tau_1), \tag{18}$$

where

$$\tau_0 = -\frac{2^{1/3}}{2 - 2^{1/3}}\Delta t \quad\text{and}\quad \tau_1 = \frac{1}{2 - 2^{1/3}}\Delta t. \tag{19}$$

TABLE I. List of abbreviations for equilibrium simulations. The propagator must be multiplied from the left by $\mathcal{R}$ for RNEMD. The generator $\mathcal{L}^D$ differs between DPD and DPDE as explained in Appendix A.

Abbreviation	Propagator	Abbreviation	Propagator
MD, VV	$\mathcal{S}_2(\Delta t)$	`MD, FS`	$\mathcal{S}_2(\tau_1)\mathcal{S}_2(\tau_0)\mathcal{S}_2(\tau_1)$
`MD, VV(p0)`	$\mathcal{P}_v\mathcal{S}_2(\Delta t)$	`MD, FS(p0)`	$\mathcal{P}_v\mathcal{S}_2(\tau_1)\mathcal{S}_2(\tau_0)\mathcal{S}_2(\tau_1)$
`MD, VV(x1)`	$e^{\mathcal{L}^E(\chi=0.01)\Delta t}\mathcal{S}_2(\Delta t)$	`MD, FS(x1)`	$e^{\mathcal{L}^E(\chi=0.01)\Delta t}\mathcal{S}_2(\tau_1)\mathcal{S}_2(\tau_0)\mathcal{S}_2(\tau_1)$
`MD, VV(x2)`	$e^{\mathcal{L}^E(\chi=0.1)\Delta t}\mathcal{S}_2(\Delta t)$	`MD, FS(x2)`	$e^{\mathcal{L}^E(\chi=0.1)\Delta t}\mathcal{S}_2(\tau_1)\mathcal{S}_2(\tau_0)\mathcal{S}_2(\tau_1)$
`MD, VV(x3)`	$e^{\mathcal{L}^E(\chi=10)\Delta t}\mathcal{S}_2(\Delta t)$	`MD, FS(x3)`	$e^{\mathcal{L}^E(\chi=10)\Delta t}\mathcal{S}_2(\tau_1)\mathcal{S}_2(\tau_0)\mathcal{S}_2(\tau_1)$
`DPD, VV`	$e^{\mathcal{L}^D\Delta t}\mathcal{S}_2(\Delta t)$	`DPD, FS`	$e^{\mathcal{L}^D\Delta t}\mathcal{S}_2(\tau_1)\mathcal{S}_2(\tau_0)\mathcal{S}_2(\tau_1)$
`DPDE, VV`	$e^{\mathcal{L}^D\Delta t}\mathcal{S}_2(\Delta t)$	`DPDE, FS`	$e^{\mathcal{L}^D\Delta t}\mathcal{S}_2(\tau_1)\mathcal{S}_2(\tau_0)\mathcal{S}_2(\tau_1)$
`DPDE, VV(p0)`	$e^{\mathcal{L}^D\Delta t}\mathcal{P}_v\mathcal{S}_2(\Delta t)$	`DPDE, FS(p0)`	$e^{\mathcal{L}^D\Delta t}\mathcal{P}_v\mathcal{S}_2(\tau_1)\mathcal{S}_2(\tau_0)\mathcal{S}_2(\tau_1)$
`DPDE, VV(p1)`	$e^{\mathcal{L}^D\Delta t}\mathcal{P}_i\mathcal{S}_2(\Delta t)$	`DPDE, FS(p1)`	$e^{\mathcal{L}^D\Delta t}\mathcal{P}_i\mathcal{S}_2(\tau_1)\mathcal{S}_2(\tau_0)\mathcal{S}_2(\tau_1)$
`DPDE, VV(x1)`	$e^{\mathcal{L}^D\Delta t}e^{\mathcal{L}^E(\chi=0.01)\Delta t}\mathcal{S}_2(\Delta t)$	`DPDE, FS(x1)`	$e^{\mathcal{L}^D\Delta t}e^{\mathcal{L}^E(\chi=0.01)\Delta t}\mathcal{S}_2(\tau_1)\mathcal{S}_2(\tau_0)\mathcal{S}_2(\tau_1)$
`DPDE, VV(x2)`	$e^{\mathcal{L}^D\Delta t}e^{\mathcal{L}^E(\chi=0.1)\Delta t}\mathcal{S}_2(\Delta t)$	`DPDE, FS(x2)`	$e^{\mathcal{L}^D\Delta t}e^{\mathcal{L}^E(\chi=0.1)\Delta t}\mathcal{S}_2(\tau_1)\mathcal{S}_2(\tau_0)\mathcal{S}_2(\tau_1)$
`DPDE, VV(x3)`	$e^{\mathcal{L}^D\Delta t}e^{\mathcal{L}^E(\chi=10)\Delta t}\mathcal{S}_2(\Delta t)$	`DPDE, FS(x3)`	$e^{\mathcal{L}^D\Delta t}e^{\mathcal{L}^E(\chi=10)\Delta t}\mathcal{S}_2(\tau_1)\mathcal{S}_2(\tau_0)\mathcal{S}_2(\tau_1)$

We implement EDD through the approximation

$$e^{\mathcal{L}^E\Delta t} \approx \prod_{(i,j)} e^{\mathcal{L}^E_{ij}\Delta t}, \tag{20}$$

where the product is over all pairs of particles and

$$\mathcal{L}^E_{ij} := -\frac{\chi f}{C_2}\mu_{ij}\theta(R_c - r_{ij})v^e_{ij}\mathbf{e}_{ij}\cdot\left(\frac{1}{m_i}\frac{\partial}{\partial \mathbf{v}_i} - \frac{1}{m_j}\frac{\partial}{\partial \mathbf{v}_j}\right). \tag{21}$$

In principle, v^e_{ij}, f, and C_2 must all be recomputed after each pairwise update of the velocities (application of $e^{\mathcal{L}^E_{ij}\Delta t}$), which requires a considerable computational effort. In practice, however, we found the energy drift to be completely eliminated when f and C_2 are updated only once during each time step, which we have done right before applying the propagator $e^{\mathcal{L}^E\Delta t}$.

For DPDE equations of motion, we employ the approximate scheme

$$e^{\mathcal{L}^D\Delta t} \approx \prod_{(i,j)} e^{\mathcal{L}^{vh}_{ij}\Delta t}e^{\mathcal{L}^{hc}_{ij}\Delta t}, \tag{22}$$

where $\mathcal{L}^{hc}_{ij}$ and $\mathcal{L}^{vh}_{ij}$ denote, respectively, the generators of heat conduction and viscous heating dynamics between a pair of particles i and j.

We still need to deduce the effect of the propagators $e^{\mathcal{L}^{hc}_{ij}\Delta t}$ and $e^{\mathcal{L}^{vh}_{ij}\Delta t}$ on the microstate, which is the subject of Appendix A. Finally, we note that the expression for $\mathcal{L}^D$ differs between DPDE and DPD. However, the propagator $e^{\mathcal{L}^D\Delta t}$ for DPDE reduces to that of DPD with suitable modifications as explained in the same Appendix.

In Table I, we list the propagators of various simulations we performed in this work along with the abbreviations used in the figures shown in Sec. VI.

V. SIMULATION

To examine the usefulness of the EDD method, we performed Monte Carlo (MC), MD, DPD, and DPDE simulations of model systems and evaluated a few equilibrium and transport properties. All of these methods should agree in regard to equilibrium properties of a given model, while there should be an agreement between DPD and DPDE regarding diffusivity and viscosity.

MC yields equilibrium properties free from any dependence on the numerical integrator or the time step of integration Δt. MD allows us to examine the effectiveness of EDD when used with RNEMD alone without the added complications of dissipative and fluctuating dynamics. DPD, which simulates systems in contact with a thermal bath, does not require EDD or a projection method to control energy drift. Thus, their effects may be discerned by comparing predictions on the same properties from DPD and DPDE.

A. Model system

The interparticle potential in model A is defined in terms of the function

$$w_A(x) = \begin{cases} (1-x)^2 & (x \leqslant 1) \\ 0 & (x > 1) \end{cases} \tag{23}$$

as

$$\phi_A(r) = \varepsilon W_A w_A(r/R_c), \tag{24}$$

where r is the interparticle distance. This is the most commonly used potential in DPD.

We note that the second derivative of ϕ_A and hence the first derivative of the conservative force are discontinuous at $r = R_c$. To examine its impact, we also performed a small set of computations using model B with a smoother potential

$$\phi(r) = \varepsilon W_B w_B(r/R_c)\ , \tag{25}$$

where w_B is the cubic spline function

$$w_B(x) = \begin{cases} 1 - 6x^2 + 6x^3 & (x \leqslant 1/2) \\ 2(1-x)^3 & (1/2 < x \leqslant 1) \\ 0 & (x > 1). \end{cases} \tag{26}$$

Adopting a system of units in which $\varepsilon = 1$ and $R_c = 1$, we set $W_A = 9.375$ and $W_B = 10$. The value of W_A is the same as in

Ref. [28]. The value of W_B was determined so that

$$\int_0^{R_c} \phi_A(r) 4\pi r^2 dr = \int_0^{R_c} \phi_B(r) 4\pi r^2 dr \tag{27}$$

based on the expectation that the physical properties of models A and B would be comparable. We set $m_i = 1$ and $c_i/k_B = c/k_B = 20$ for all i so that the system is made of a single component. Following Ref. [28], $\sigma = 3$. Finally, $\alpha = 1$.

In accordance with a common practice, we use

$$\omega_{ij} = \begin{cases} 1 - r_{ij}/R_c & \text{if } r_{ij} \leqslant R_c \\ 0 & \text{otherwise} \end{cases} \tag{28}$$

for the weighting function specifying the range of the dissipative and fluctuating forces.

We used a rectangular box with height 6 and the square base of side $L = 5$, and imposed periodic boundary conditions in all three directions. The box contained $N = 600$ particles so that the particle number density was 4. The system may not be large enough to eliminate various finite-size effects, but it is expected to be sufficient for illustrating the usefulness of the method.

B. Energy

For projection methods and EDD, we must specify the target value E_0 for the total energy of the system so as to achieve a desired temperature T_0. In the simulations reported in this article, $k_B T_0 = 1$. For this purpose, we first computed the potential energy U by means of canonical ensemble MC. Then, we set

$$E_0 = U + \tfrac{3}{2} k_B T_0 (N - 1) \tag{29}$$

for MD.

According to Ref. [34], the probability distribution $p(\epsilon)$ for the internal energy ϵ of a particle in a canonical ensemble is given by

$$p(\epsilon) = \frac{\epsilon^{c/k_B} e^{-\epsilon/k_B T_0}}{(k_B T_0)^{c/k_B+1} \Gamma(c/k_B + 1)}, \tag{30}$$

where Γ denotes the gamma function. This gives

$$\langle \epsilon \rangle = k_B T_0 \left(\frac{c}{k_B} + 1 \right), \tag{31}$$

suggesting that we set

$$E_0 = U + \frac{3}{2}(N - 1) k_B T_0 + N k_B T_0 \left(\frac{c}{k_B} + 1 \right) \tag{32}$$

for DPDE.

Even though MD and DPDE simulations lead to a microcanonical as opposed to a canonical ensemble, E_0 determined by Eqs. (29) or (32) resulted in the desired temperature. A noticeable deviation was observed with the largest Δt and the smallest χ we used. While it may be possible to achieve the desired system temperature by adjusting E_0, this would prevent us from evaluating the effect of χ on the same footing and we have used the same E_0 value throughout ($E_0 = 27.818$ for model A and $E_0 = 26.678$ for model B).

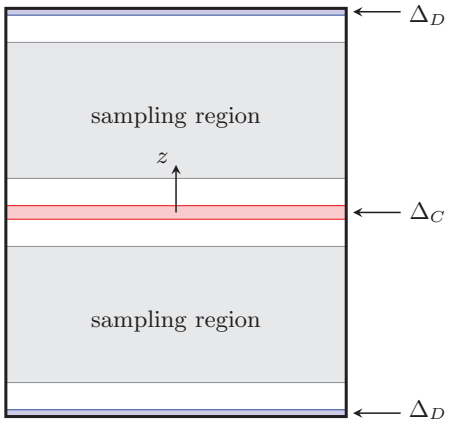

FIG. 1. Swap regions (Δ_C and Δ_D) and the sampling regions in the simulation box.

C. Transport properties

Diffusivity was computed using the mean-square displacement of particles in equilibrium simulations, while viscosity and thermal conductivity were computed using reverse nonequilibrium molecular dynamics (RNEMD) [15]. For this purpose, we choose two thin parallel swap regions Δ_C and Δ_D in the simulation box. In a coordinate system with its origin at the center of the simulation box and the z axis perpendicular to two of the opposing square faces of the box, they are defined by $|z| \leqslant 0.1$ and $|z| \geqslant 2.9$, respectively. Figure 1 provides a schematic representation of the simulation box.

For viscosity calculation, we first identify a particle with the smallest x component (p_{xC}) of the momentum in region Δ_C and a particle with the largest x component (p_{xD}) of the momentum in region Δ_D. Then, we assign p_{xD} and p_{xC} to the first and the second particles, respectively. This results in the transfer of momentum in the amount of $p_{xD} - p_{xC}$ from region Δ_D to Δ_C. This momentum then flows back to region Δ_D in the form of viscous momentum flux driven by the velocity gradient du_x/dz. On average, the swap move was performed at the rate of 0.75 times per unit time both in MD and in DPD(E). This frequency was chosen so that a linear velocity profile, $u_x(z)$, is established outside regions Δ_C and Δ_D. The slope du_x/dz was estimated by least square fitting of a line to the velocity profile in the sampling region defined by $0.5 \leqslant |z| \leqslant 2.5$. The viscosity μ is then evaluated as

$$\mu = -\frac{\sum (p_{xD} - p_{xC})/(2\tau L^2)}{du_x/dz}, \tag{33}$$

where the sum is over all swap moves performed during the entire duration τ of the simulation. The factor of 2 in Eq. (33) accounts for the fact that, under the periodic boundary conditions, the momentum flows from region Δ_C to region Δ_D in both the positive and negative z directions.

For thermal conductivity calculation, we identify a particle with the smallest kinetic energy ($m_C {v_C}^2/2$) in region Δ_C and a particle with the largest kinetic energy ($m_D {v_D}^2/2$) in region Δ_D. Then, we swap the velocity vectors of these particles. The swap move was performed at the rate of 0.75 and 2.5 times per unit time in MD and in DPDE, respectively. This induces

a heat flux in the z direction

$$q_z = \sum \left(m_D v_D^2/2 - m_C v_C^2/2\right)/(2\tau L^2), \tag{34}$$

in which the sum is over all swap moves performed during the simulation.

In the case of MD combined with RNEMD, the thermal conductivity is given by

$$\kappa = -\frac{q_z}{d(k_B T_k)/dz}, \tag{35}$$

where

$$k_B T_k(z) := \frac{N}{N-1}\left\langle \frac{m}{3N_\delta} \sum \left({v_x}^2 + {v_y}^2 + {v_z}^2\right)\right\rangle \tag{36}$$

is the dimensionless temperature profile based on the kinetic energy of particles. In this expression, N_δ is the number of particles within a slab of thickness $\delta = 0.01$ centered at z and the sum is only over these particles. The factor $N/(N-1)$ ensures that the volume average of $k_B T_k(z)$ agrees with $k_B T_k$ defined by Eq. (43) below for a uniform system.

In DPDE, the temperature profile may also be computed using the internal energy of the particles as

$$k_B T_i(z) := \left\langle \frac{1}{N_\delta} \sum_i \frac{c}{\epsilon_i} \right\rangle^{-1}. \tag{37}$$

The σ value we used did not allow for an efficient energy exchange between the translational and internal degrees of freedom of the particles in comparison to the energy exchange among the latter degrees of freedom alone, the process whose rate is determined by α. This led to a noticeable discrepancy between $k_B T_k(z)$ and $k_B T_i(z)$. As shown in Fig. 12 below, the temperature profiles are well described by the following seven parameter model including κ_k and κ_i, referring, respectively, to the thermal conductivity associated with energy exchange among particles through their translational and internal degrees of freedom:

$$\begin{aligned} k_B T_k(\zeta) &= \frac{1}{\kappa_t}[\Theta(\zeta) + \kappa_i \Delta(\zeta)], \\ k_B T_i(\zeta) &= \frac{1}{\kappa_t}[\Theta(\zeta) - \kappa_k \Delta(\zeta)], \end{aligned} \tag{38}$$

where

$$\begin{aligned} \Delta(\zeta) &:= k_B T_k(\zeta) - k_B T_i(\zeta) \\ &= A_1 \cosh(a\zeta) + A_2 \sinh(a\zeta) + \frac{\Phi}{\lambda}, \\ \Theta(\zeta) &:= \kappa_k k_B T_k(\zeta) + \kappa_i k_B T_i(\zeta) = -q_z \zeta + A_3, \end{aligned} \tag{39}$$

and the ζ axis points in the same direction as the z axis but its origin is at the center of the sampling region. In these equations, $A_1, A_2, A_3, a, \Phi/\lambda, \kappa_k$, and κ_i are model parameters to be determined, and $\kappa_t := \kappa_k + \kappa_i$. Finally, q_z is directly measurable in RNEMD simulations.

Using the Levenberg-Marquardt method [35], we first fit $\Delta(z)$ to the temperature profiles from a simulation to determine A_1, A_2, a, and Φ/λ, and then $T_i(z)$ to determine κ_k/κ_t, q_z/κ_t, and A_3/κ_t, from which the values for κ_k and κ_i can be determined.

D. Energy drift

In the absence of EDD moves, Eq. (11) reduces to

$$df = Adt + BdW. \tag{40}$$

This gives

$$E_w\{f(t)\} = At \quad \text{and} \quad E_w\{[f(t) - E_w\{f(t)\}]^2\} = B^2 t, \tag{41}$$

where $E_w\{\cdot\}$ denotes the average over all possible realization of the stochastic noise. To the extent that Eq. (40) describes the behavior of f adequately, the energy drift is unbounded even if $A = 0$. In contrast, Eq. (12) indicates that

$$E_w\{[f(t) - E_w\{f(t)\}]^2\} = \frac{B^2}{\chi} = \text{constant} \tag{42}$$

with EDD.

E. Additional details of simulations

We examined six values for the time step of integration: $\Delta t = 0.002$, 0.01, 0.02, 0.04, 0.08, and 0.1. Each MD or DPD(E) simulation involved an equilibration over the time duration of 4×10^3 and sampling over the time duration of 6.4×10^4–1.6×10^5. MD and DPDE without any control over the energy drift were exceptions. These trajectories were generated using, as the initial condition, a well-equilibrated system under the projection method with velocity rescaling. MC simulations consisted of 2×10^5 and 4×10^6 MC steps for equilibration and sampling, respectively. We generated 16 independent trajectories for each simulation conditions. Each physical property was obtained as the average over these independent trajectories. In the figures below, we will omit error bars if they are smaller than the size of the symbols indicating the average, or if they are visible only in the lower portion of a logarithmic plot.

VI. RESULTS

In what follows, we will omit results from EDD with $\chi = 0.1$ (x2 in the abbreviation in Table I) and projection methods (p0 and p1) as they are nearly identical to those from EDD with $\chi = 10$ (x3). The Supplemental Material provides a more complete set of results [36].

A. Equilibrium properties

In Fig. 2, we show the dependence of the kinetic-energy-based system temperature

$$k_B T_k := \left\langle \frac{1}{3(N-1)} \sum_i m_i \|\mathbf{v}_i\|^2 \right\rangle \tag{43}$$

on the time step of integration Δt in equilibrium DPD simulations. We note that when VV is used to integrate the conservative dynamics, the smoother interparticle potential energy (model B) actually gives a slightly larger deviation of $k_B T_k$ from the set value ($k_B T_0 = 1$) compared to the less smooth potential energy (model A). In complete agreement with Ref. [28], however, a significant reduction in the deviation was observed when the conservative dynamics is integrated using the fourth-order symplectic method (FS) for

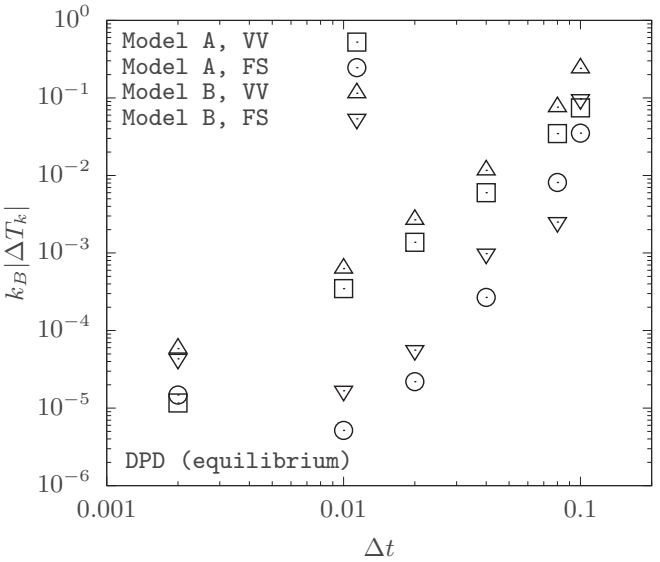

FIG. 2. The time-step dependence of the kinetic temperature T_k in DPD simulations at $k_BT_0 = 1$. $\Delta T_k := T_k - T_0$.

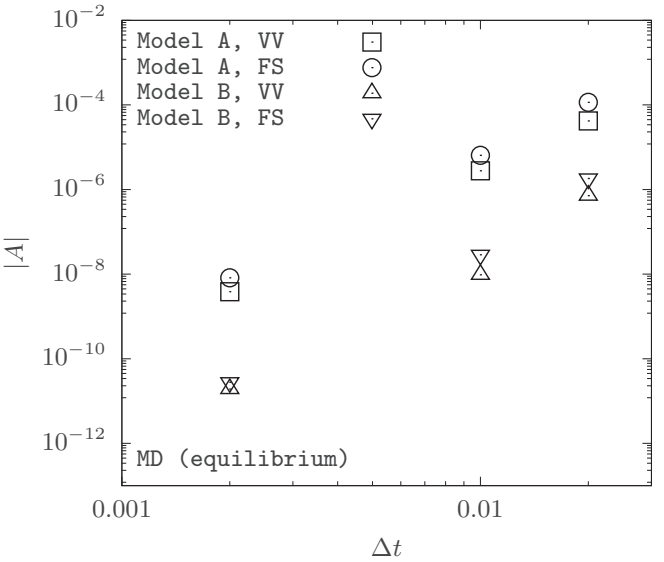

FIG. 4. Dependence on Δt of the rate of energy drift in equilibrium MD simulations.

both model potentials. The same applies to other equilibrium properties [36].

To examine how the integrator affects the conservative dynamics, we performed MD simulations on model A without any thermostat. Figure 3 shows the time evolution of

$$\Delta e_n(\tau) := \langle \overline{e_n}(\tau) - \overline{e_n}(\delta\tau) \rangle, \tag{44}$$

where $e_n := E/N$ and $\overline{e_n}(\tau)$ is a short time average of e_n between time $\tau - \delta\tau$ and τ with $\delta\tau = 4$, and the angular brackets indicate the average over 16 independent trajectories. A significant energy drift is observed for $\Delta t \geqslant 0.01$ with FS, which is much larger than with VV.

Clearly, the significant improvement in the equilibrium properties, such as k_BT_k in Fig. 2, arises *not* from FS used in isolation but from FS used *in combination with* the dissipative and fluctuating pairwise dynamics of DPD, which is serving as a thermostat to counter the energy drift caused by using either a large Δt or a not sufficiently smooth potential. This interplay between the integrator of conservative dynamics and the dissipative and fluctuating dynamics is also observed in DPDE. Based on Eq. (41), we estimated the rate of energy drift A by fitting a line to $\Delta e_n(\tau)$ from simulations. It is clear from Fig. 3 that $\Delta e_n(\tau)$ can increase more rapidly than is implied by the linear relation. In such cases, we computed A from a short initial portion of the trajectories. The results are shown in Figs. 4 and 5 for equilibrium MD and DPDE simulations, respectively. A comparison of these two figures reveals that the dissipative and fluctuating dynamics affects $|A|$ more if VV is used. This is seen with both model potentials, but the

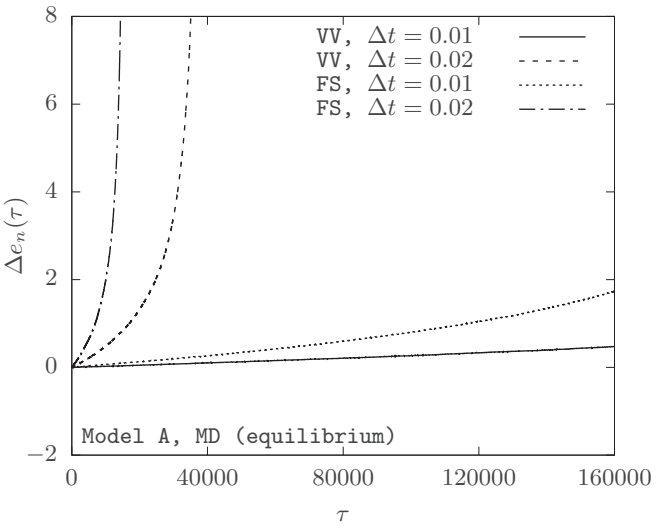

FIG. 3. Drift in total energy per particle in equilibrium molecular dynamics simulations of model A.

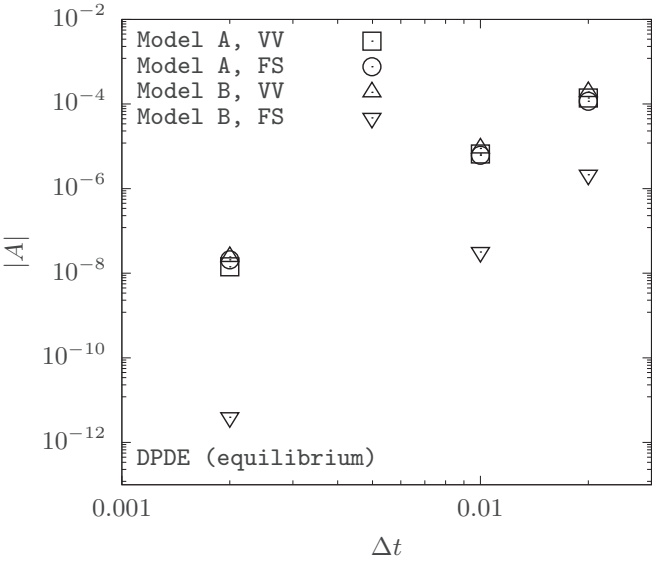

FIG. 5. Dependence on Δt of the rate of energy drift in equilibrium DPDE simulations.

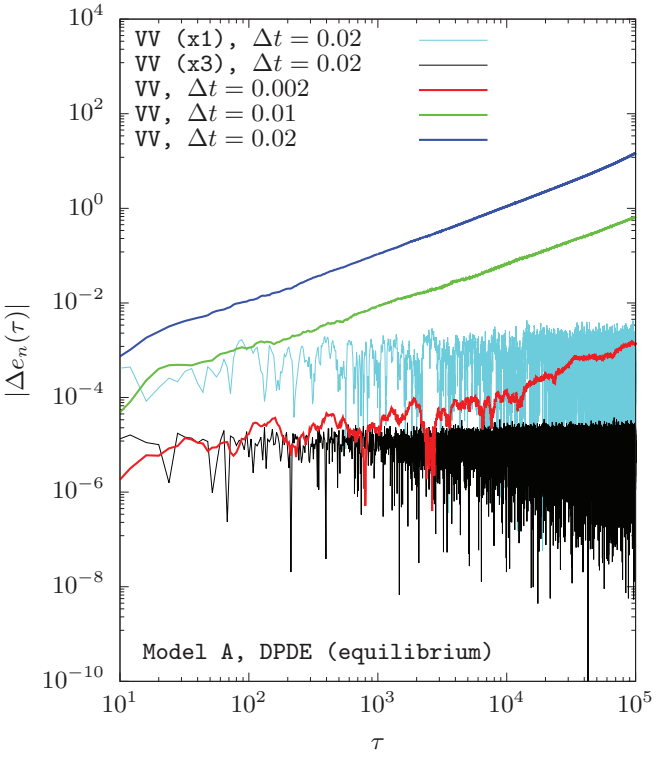

FIG. 6. Drift of the total energy per particle as characterized by $\Delta e_n(\tau)$ in equilibrium DPDE simulations of model A.

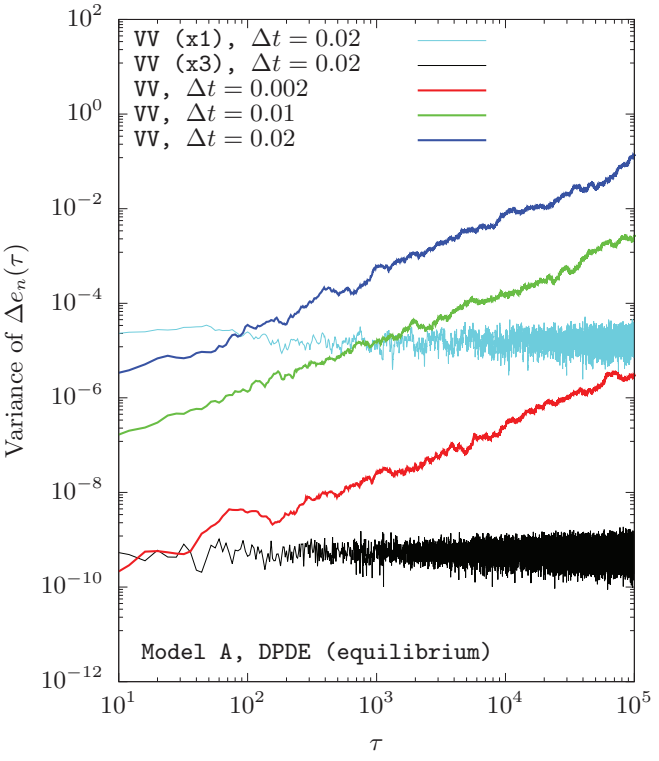

FIG. 7. Variance of the drift $\Delta e_n(\tau)$ of the total energy per particle in equilibrium DPDE simulations of model A.

effect is more pronounced for model B. When measured in terms of $|A|$, FS does not offer a clear advantage over VV for DPDE of model A.

We also note that $|A|$ values in DPDE for model A are comparable to the corresponding values in MD. It is thus clear from Fig. 3 that, if one insists on using model A and a time step as large as $\Delta t \geqslant 0.01$ and still wishes to perform a long time simulation as is needed in estimating transport properties, some measure of controlling the energy drift is essential. Accordingly, MD and DPDE simulations with $\Delta t \geqslant 0.04$ were all performed with either projection method or EDD in place.

Figures 6 and 7 demonstrate the effectiveness of EDD in controlling the energy drift. In particular, both $|\Delta e_n(\tau)|$ and its variance remain constant if EDD is applied. The figures might invoke an impression to the contrary only because data points are more densely placed toward the right of the figures.

In Fig. 8, we show the Δt dependence of the kinetic temperature $k_B T_k$ in DPDE simulations with E_0 set by Eq. (32). The results are comparable to those from DPD in Fig. 2. Thus, we conclude EDD in DPDE plays a role similar to the thermostat in DPD in that they both control the system temperature equally well while preventing the energy drift when a large Δt is used. In contrast to DPD, however, EDD leads to a microcanonical ensemble. We also note that the deviation $k_B|\Delta T_k|$ can be reduced significantly using FS in place of VV but to a lesser extent compared to DPD.

The radial distribution function $g(r)$ at small r values also shows a small but systematic Δt dependence. To quantify the error, we obtained the radial distribution function $g_{\mathrm{dpd(e)}}(r)$ and $g_{\mathrm{mc}}(r)$ from DPD(E) and MC simulations, respectively, and computed

$$\int \left| \frac{g_{\mathrm{dpd(e)}}(r)}{g_{\mathrm{mc}}(r)} - 1 \right| dr. \tag{45}$$

The usual factor of r^2 was not included in the integral in order to emphasize the contribution from small r values. The

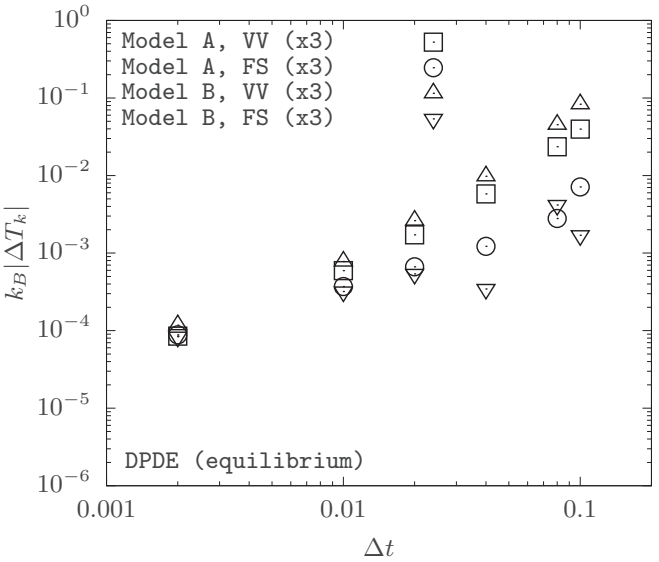

FIG. 8. The time-step dependence of the kinetic temperature T_k in DPDE simulations with EDD. $\Delta T_k := T_k - T_0$ with $k_B T_0 = 1$.

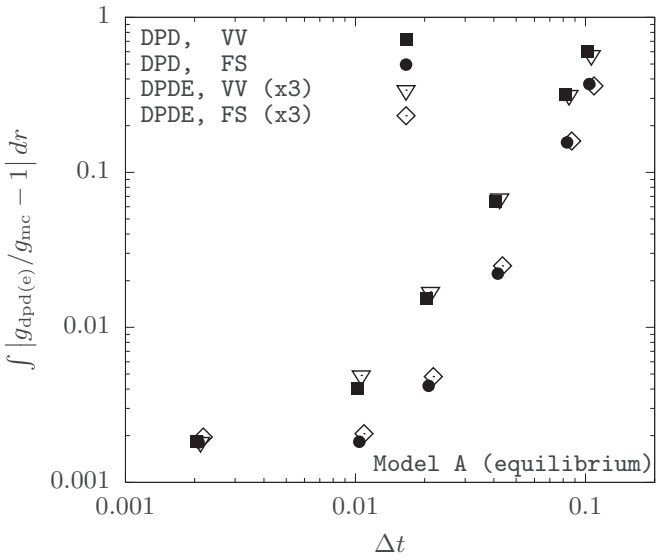

FIG. 9. Dependence on Δt of the integrated error in the radial distribution function. To improve visibility, points are shifted to the right from one data set to another in the increment of $0.02 \times \Delta t$.

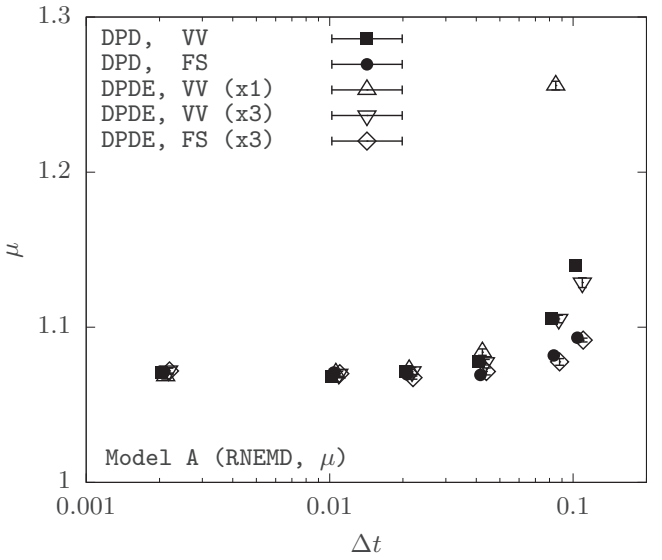

FIG. 11. Dependence on Δt of the viscosity in DPD(E) simulations with RNEMD moves. To improve visibility, points are shifted to the right from one data set to another in the increment of $0.02 \times \Delta t$.

result is shown in Fig. 9. As with other equilibrium properties, the error is smaller if a smaller Δt is used. The use of FS in place of VV reduces the error significantly especially for $\Delta t \geqslant 0.01$. We note that DPD and DPDE give rise to Δt dependence of a comparable magnitude for this quantity.

The Δt dependence of other equilibrium properties are reported in Ref. [36], further reaffirming much of the observations we have made here.

B. Transport properties

As shown in Figs. 10 and 11, both diffusivity and viscosity from DPDE (with EDD, $\chi = 10$) are in excellent agreement with the corresponding quantities of DPD up to $\Delta t = 0.08$, thus indicating that EDD introduces no artificial effect on the transport properties, either.

EDD with $\chi = 0.01$ (x1) with E_0 given by Eq. (32), while still eliminating the secular energy drift, fails to achieve the desired temperature $k_B T_0 = 1$ for $\Delta t \geqslant 0.08$, thus leading to a larger discrepancy from the corresponding DPD value and sometimes resulting in the values falling outside the field of vision in some of the figures. This is expected: According to Eq. (12), the average value of f, the deviation per particle of the system energy from the set value E_0/N, is A/χ. This quantity increases with decreasing χ and, as Figs. 4 and 5 indicate, increases with increasing Δt through the dependence of A on Δt.

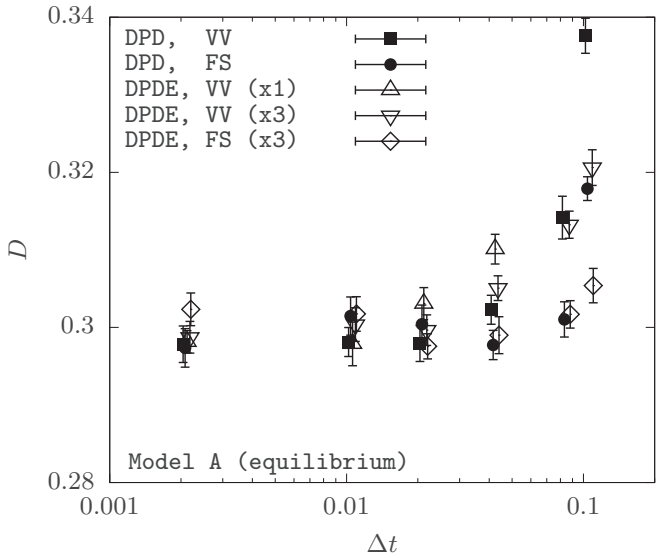

FIG. 10. Dependence on Δt of the diffusivity in equilibrium DPD(E) simulations. To improve visibility, points are shifted to the right from one data set to another in the increment of $0.02 \times \Delta t$.

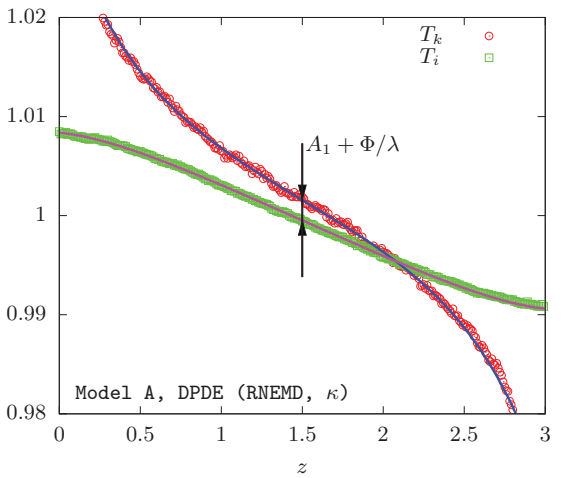

FIG. 12. Temperature profiles in a DPDE simulation with RNEMD moves for thermal conductivity calculation. Lines are the fits based on Eq. (38) to data in the range $0.5 \leqslant z \leqslant 2.5$.

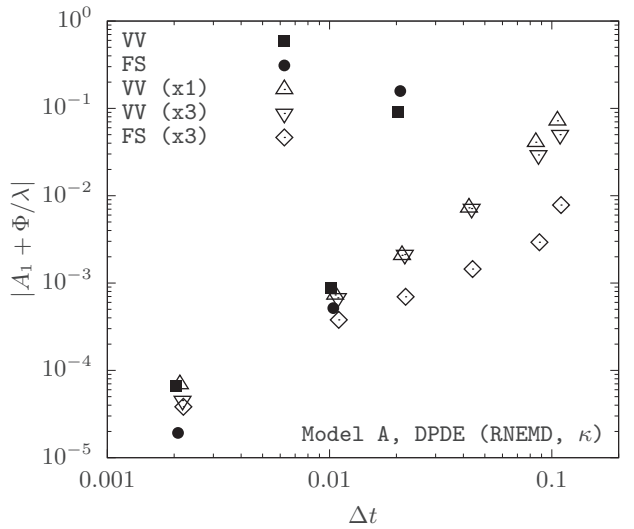

FIG. 13. Dependence on Δt of a systematic error in steady-state temperature profiles as characterized by $A_1 + \Phi/\lambda$. To improve visibility, points are shifted to the right from one data set to another in the increments of $0.02 \times \Delta t$.

We also note that both D and μ are nearly independent of Δt up to $\Delta t = 0.04$, but they start to increase with increasing Δt beyond this value. From the figures, we observe that FS performs somewhat better in this regard.

The viscosity values we found with DPD(E) are not substantially larger than the values ($\approx$0.995) from MD [36]. This implies that the viscous heating, the only mechanism of energy exchange between the translational and internal degrees of freedom, is rather weak. Figure 12 shows the temperature profiles from a DPDE simulation using $\Delta t = 0.02$ with RNEMD moves for thermal conductivity computation. As expected, a noticeable discrepancy exists between $k_B T_k(z)$ and $k_B T_i(z)$. The discrepancy does not diminish even when a smaller Δt is used. Nonetheless, Eq. (38) represents the simulation data very well.

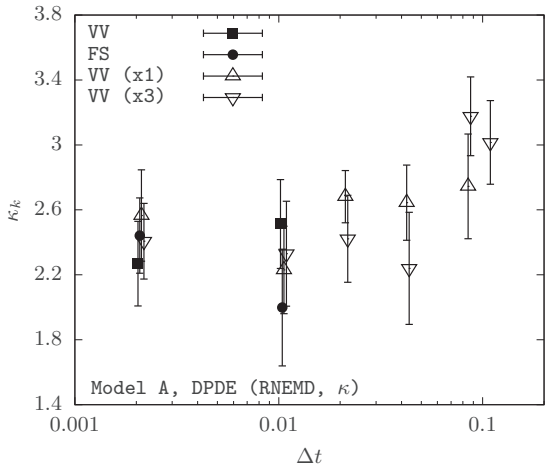

FIG. 14. Dependence on Δt of the thermal conductivity κ_k due to the translational degrees of freedom of particles. DPDE simulations with RNEMD moves. To improve visibility, points are shifted to the right from one data set to another in the increments of $0.02 \times \Delta t$.

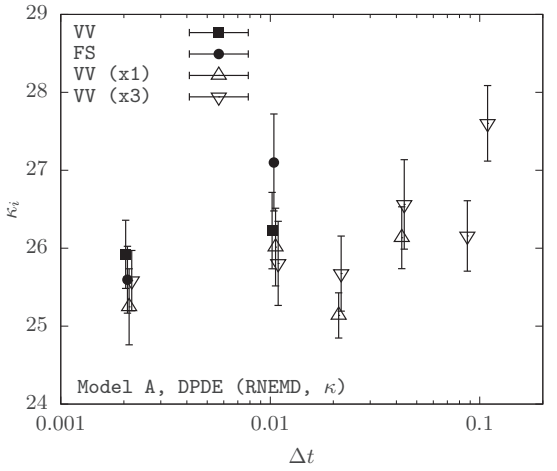

FIG. 15. Dependence on Δt of the thermal conductivity κ_i due to the internal degrees of freedom of particles. DPDE simulations with RNEMD moves. To improve visibility, points are shifted to the right from one data set to another in the increments of $0.02 \times \Delta t$.

On the basis of symmetry, it may be argued that $A_1 + \Phi/\lambda = 0$ at the center of the sampling region ($z = 1.5$ and $\zeta = 0$). As seen in Figs. 12 and 13, however, this is not the case, indicating that a large Δt leads to a systematic error in the steady-state temperature profiles. Nevertheless, the error is seen to be still very small and can be reduced when FS is used. Moreover, as shown in Figs. 14 and 15, the thermal conductivities κ_k and κ_i we found are, within statistical errors, independent of Δt up to $\Delta t = 0.04$. Simulations without a proper energy control measure manifestly fail to give convergent results for κ_k and κ_i if $\Delta t = 0.02$ is used, and hence the data are not included in these figures.

VII. CONCLUSION

We demonstrated that EDD completely eliminates the secular energy drift in DPDE and RNEMD, thus allowing for a simulation of a long enough duration to compute various transport properties. EDD remains effective even when an interparticle potential is not sufficiently smooth or when a larger Δt is used. The method introduces no discernible artifact to equilibrium or transport properties of the model systems we studied.

EDD achieves this by imposing a small perturbation on the projected relative velocities for each pair of particles. In this way, it ensures the exact conservation of the total linear momentum and does not rely on the particles having internal degrees of freedom. This is in contrast to the existing projection methods in which either velocities or internal energies of particles are adjusted.

The actual size of the energy fluctuation ΔE, which is controlled through the parameter χ, has no noticeable effects on any of equilibrium properties or transport coefficients we computed when $\chi \geqslant 0.1$. Insofar as EDD leads to microcanonical ensemble, this is expected for the former. However, that the same applies to the latter is worth emphasizing. The

dependence on χ became apparent when a smaller value ($\chi = 0.01$) was used. This is due to the inability of EDD to achieve the desired temperature if χ is too small and E_0 is determined by Eq. (32). Even then, EDD successfully eliminated the energy drift for all time step sizes we considered.

The energy drift originates from the integration scheme for the primary dynamics, and the numerical error of the integrator is expected to affect both velocities and positions of the particles. In EDD, however, the error is counteracted only through particle velocities. Thus, the use of EDD introduces a tacit assumption of an efficient and correct repartitioning of the system energy between kinetic and potential energy components within relevant timescales of a phenomenon under consideration. The energy that needs to be repartitioned is expected to increases with increasing Δt, and this explains the systematic Δt dependence we observed in many of the equilibrium and transport properties. Our integration scheme for DPDE is based on SSA. Not surprisingly, therefore, the Δt dependence we observed is comparable to what is seen with the standard implementation of isothermal DPD, which is also based on SSA.

EDD and the projection methods we considered are equally effective in eliminating the energy drift. However, the use of the pairwise dynamics makes EDD structurally similar to the DPD thermostat, suggesting that underlying ideas of a more recent advance in DPD [27] might be transferable to DPDE. We emphasize, however, that EDD differs from the DPD thermostat in that it leads to (nearly) constant energy trajectories and allows for a steady state with a nonuniform temperature field.

In complete agreement with the recent study on DPD [28], in DPDE also, the Δt dependence of various equilibrium and transport properties can be reduced considerably by using FS instead of VV. Interestingly, however, this does *not* imply that the energy is better conserved by FS. In fact, the energy diverges more rapidly for MD of model A if FS is used in place of VV.

VV and FS algorithms are microscopically reversible and conserve the phase volume. Because the velocity update scheme Eq. (13) arises from a dissipative force, this is not the case with EDD. Nevertheless, EDD leads to microcanonical distribution and hence (by itself) does not introduce any distortion on the equilibrium properties if the additional assumption of ergodicity is made. The goal of EDD is to suppress energy drifts in DPDE or RNEMD. Neither possesses microscopic reversibility, DPDE due to the dissipative and fluctuating forces and RNEMD due to dynamics driven by Maxwell's demon.

We considered two potential issues with EDD: (1) if it affects transport properties and (2) if the approximation of updating C_2 only once per time step leads to any systematic errors. Comparing both equilibrium and transport properties estimated with EDD against those without EDD (but using MC, DPD, or DPDE with small Δt), we observed no detectable consequence stemming from these potential issues.

EDD introduces an explicit coupling between each particle pair and the state of the entire system as characterized by f. Further investigation is needed to examine how these aspects of EDD might impact other equilibrium properties, hydrodynamics, and transient behavior especially in nonuniform systems (such as heat conduction from one region to another).

In DPDE, temperature may be computed from either kinetic or internal energy of particles. For some combinations of σ and α, a discrepancy may arise in nonisothermal simulations between these two temperatures due to inefficient energy exchange between translational and internal degrees of freedom of particles. We have shown how thermal conductivity can nevertheless be estimated by combining two distinct temperature profiles across the system. In principle, this same issue can affect different energy controlling measures differently, i.e., the projection method by means of velocity rescaling and EDD on the one hand and the projection method with internal energy rescaling on the other. Nevertheless, the physical properties we examined did not show statistically significant differences among these methods.

ACKNOWLEDGMENT

Computations reported here were made possible by a resource grant from the Ohio Supercomputer Center [37].

APPENDIX A: INTEGRATION OF DPDE EQUATIONS OF MOTION

Written for each pair of particles i and j, the equations of motion for the dissipative and fluctuating dynamics of DPDE are given by

$$d\mathbf{v}_i = -\frac{\gamma_{ij}}{m_i}\omega_{ij}{}^2 v_{ij}^e \mathbf{e}_{ij} dt + \frac{\sigma}{m_i}\omega_{ij}\mathbf{e}_{ij} \circ dW_{ij}^v, \quad \text{(A1a)}$$

$$d\mathbf{v}_j = \frac{\gamma_{ij}}{m_j}\omega_{ij}{}^2 v_{ij}^e \mathbf{e}_{ij} dt - \frac{\sigma}{m_j}\omega_{ij}\mathbf{e}_{ij} \circ dW_{ij}^v, \quad \text{(A1b)}$$

$$d\epsilon_i = \frac{1}{2}\left[\gamma_{ij} v_{ij}^e{}^2 + \alpha^2\left(\frac{c_i}{\epsilon_i} - \frac{c_j}{\epsilon_j}\right)\right]\omega_{ij}{}^2 dt - \frac{1}{2}\sigma\omega_{ij} v_{ij}^e \circ dW_{ij}^v + \alpha\omega_{ij} \circ dW_{ij}^\epsilon, \quad \text{(A1c)}$$

$$d\epsilon_j = \frac{1}{2}\left[\gamma_{ij} v_{ij}^e{}^2 - \alpha^2\left(\frac{c_i}{\epsilon_i} - \frac{c_j}{\epsilon_j}\right)\right]\omega_{ij}{}^2 dt - \frac{1}{2}\sigma\omega_{ij} v_{ij}^e \circ dW_{ij}^v - \alpha\omega_{ij} \circ dW_{ij}^\epsilon. \quad \text{(A1d)}$$

We split the pairwise stochastic dynamics Eq. (A1) into two subdynamics: the heat conduction dynamics and the viscous heating dynamics. The former affects the internal energy of particles only and is given by

$$d\epsilon_i = -d\epsilon_j = \frac{1}{2}\alpha^2\left(\frac{c_i}{\epsilon_i} - \frac{c_j}{\epsilon_j}\right)\omega_{ij}{}^2 dt + \alpha\omega_{ij} \circ dW_{ij}^\epsilon. \quad \text{(A2)}$$

The latter affects both velocity and internal energy of particles and is described by Eqs. (A1a), (A1b), and

$$d\epsilon_i = d\epsilon_j = \tfrac{1}{2}\gamma_{ij}\omega_{ij}{}^2 v_{ij}^e{}^2 dt - \tfrac{1}{2}\sigma\omega_{ij} v_{ij}^e \circ dW_{ij}^v. \quad \text{(A3)}$$

Treating ϵ_i and ϵ_j on the right-hand side of Eq. (A2) as if they are constant, we integrate Eq. (A2) over the time duration Δt:

$$\Delta\epsilon_i = -\Delta\epsilon_j = \frac{1}{2}\alpha^2\left(\frac{c_i}{\epsilon_i} - \frac{c_j}{\epsilon_j}\right)\omega_{ij}{}^2 \Delta t + \alpha\omega_{ij}\xi\sqrt{\Delta t}, \quad \text{(A4)}$$

where ξ is a random number taken from the normal distribution $N(0, 1)$. This gives the updating scheme for the heat conduction dynamics.

We now turn to the updating scheme for the viscous heating dynamics. Subtracting Eq. (A1b) from (A1a) and taking the dot product between the resulting equation and $\mathbf{e}_{ij}$, we find

$$dv_{ij}^e = -\frac{\gamma_{ij}}{\mu_{ij}}\omega_{ij}{}^2 v_{ij}^e dt + \frac{\sigma}{\mu_{ij}}\omega_{ij} \circ dW_{ij}^v. \tag{A5}$$

Under the same approximation of treating ϵ_i and ϵ_j (in γ_{ij}) as constant, we can integrate Eq. (A5) by a method similar to what is used in Refs. [38,39]. This gives [12]

$$\Delta v_{ij}^e = (e^{-d_{ij}\Delta t} - 1)v_{ij}^e + \frac{\sigma\omega_{ij}}{\mu_{ij}}\xi\sqrt{\frac{1}{2d_{ij}}(1 - e^{-2d_{ij}\Delta t})}, \tag{A6}$$

where

$$d_{ij} := \frac{\gamma_{ij}\omega_{ij}{}^2}{\mu_{ij}}. \tag{A7}$$

For large values of σ, the approximation made here can lead to a systematic discrepancy between the kinetic-energy-based temperature Eq. (43) and the internal-energy-based temperature

$$k_B T_i = \left\langle \frac{1}{N}\sum_i \frac{c_i}{\epsilon_i} \right\rangle^{-1}. \tag{A8}$$

The error can be reduced, however, if a smaller time step is used in Eq. (A6).

Equation (A6) may be approximated as

$$\begin{aligned}\Delta v_{ij}^e &\approx \left(-d_{ij}v_{ij}^e\Delta t + \frac{\sigma\omega_{ij}}{\mu_{ij}}\xi\sqrt{\Delta t}\right)\left(1 - \frac{1}{2}d_{ij}\Delta t\right) \\ &\approx \frac{1}{1 + d_{ij}\Delta t/2}\left(-d_{ij}v_{ij}^e\Delta t + \frac{\sigma\omega_{ij}}{\mu_{ij}}\xi\sqrt{\Delta t}\right).\end{aligned} \tag{A9}$$

As shown in Appendix B, Eq. (A9) is equivalent to the update scheme for viscous heating dynamics developed in Ref. [11], and we used Eq. (A9) in this work. The difference between Eqs. (A6) and (A9) is of the order of $(\Delta t)^{5/2}$.

From Eqs. (A1a) and (A1b), it readily follows that $m_i d\mathbf{v}_i + m_j d\mathbf{v}_j = \mathbf{0}$ and that both $d\mathbf{v}_i$ and $d\mathbf{v}_j$ are parallel to $\mathbf{e}_{ij}$. Since $\mathbf{e}_{ij}$ remains unaffected by the subdynamics under consideration, $dv_{ij}^e = d(\mathbf{e}_{ij}\cdot\mathbf{v}_{ij}) = \mathbf{e}_{ij}\cdot(d\mathbf{v}_i - d\mathbf{v}_j)$. Thus,

$$d\mathbf{v}_i = \frac{\mu_{ij}}{m_i}\mathbf{e}_{ij}dv_{ij}^e \quad \text{and} \quad d\mathbf{v}_j = -\frac{\mu_{ij}}{m_j}\mathbf{e}_{ij}dv_{ij}^e \tag{A10}$$

and hence the update scheme for the velocities is

$$\Delta\mathbf{v}_i = \frac{\mu_{ij}}{m_i}\mathbf{e}_{ij}\Delta v_{ij}^e \quad \text{and} \quad \Delta\mathbf{v}_j = -\frac{\mu_{ij}}{m_j}\mathbf{e}_{ij}\Delta v_{ij}^e. \tag{A11}$$

From Eqs. (A1a), (A1b), and (A3),

$$d\epsilon_i = d\epsilon_j = -\tfrac{1}{2}d(K_i + K_j), \tag{A12}$$

indicating that the viscous heating dynamics conserves energy. Thus,

$$\begin{aligned}\Delta\epsilon_i = \Delta\epsilon_j &= -\tfrac{1}{2}\Delta(K_i + K_j) \\ &= -\tfrac{1}{2}\mu_{ij}\Delta v_{ij}^e\left(v_{ij}^e + \tfrac{1}{2}\Delta v_{ij}^e\right).\end{aligned} \tag{A13}$$

Note that the propagator $e^{\mathcal{L}^D\Delta t}$ for DPDE reduces to that of DPD by omitting the updating schemes Eqs. (A4) and (A13), and then setting $c_i/\epsilon_i = c_j/\epsilon_j = 1/k_BT$ when evaluating γ_{ij} in Eq. (A7).

APPENDIX B: VISCOUS HEATING DYNAMICS

In the notation we have been using in this article, Eqs. (11a)–(11d) of Ref. [11] read

$$\mathbf{v}_i(\Delta t/2) = \mathbf{v}_i(0) - \frac{\Delta t}{2m_i}\gamma_{ij}\omega_{ij}{}^2 v_{ij}^e(0)\mathbf{e}_{ij} + \frac{\sqrt{\Delta t}}{2m_i}\sigma\omega_{ij}\xi\mathbf{e}_{ij}, \tag{B1a}$$

$$\mathbf{v}_j(\Delta t/2) = \mathbf{v}_j(0) + \frac{\Delta t}{2m_j}\gamma_{ij}\omega_{ij}{}^2 v_{ij}^e(0)\mathbf{e}_{ij} - \frac{\sqrt{\Delta t}}{2m_j}\sigma\omega_{ij}\xi\mathbf{e}_{ij}, \tag{B1b}$$

$$\begin{aligned}\mathbf{v}_i(\Delta t) = \mathbf{v}_i(\Delta t/2) &- \frac{\Delta t}{2m_i}\gamma_{ij}\omega_{ij}{}^2 v_{ij}^e(\Delta t)\mathbf{e}_{ij} \\ &+ \frac{\sqrt{\Delta t}}{2m_i}\sigma\omega_{ij}\xi\mathbf{e}_{ij},\end{aligned} \tag{B1c}$$

$$\begin{aligned}\mathbf{v}_j(\Delta t) = \mathbf{v}_j(\Delta t/2) &+ \frac{\Delta t}{2m_j}\gamma_{ij}\omega_{ij}{}^2 v_{ij}^e(\Delta t)\mathbf{e}_{ij} \\ &- \frac{\sqrt{\Delta t}}{2m_j}\sigma\omega_{ij}\xi\mathbf{e}_{ij},\end{aligned} \tag{B1d}$$

Subtracting Eq. (B1b) from Eq. (B1a) and taking the dot product between $\mathbf{e}_{ij}$ and the resulting equation, we find

$$v_{ij}^e(\Delta t/2) = v_{ij}^e(0) - d_{ij}v_{ij}^e(0)\frac{\Delta t}{2} + \frac{\sigma\omega_{ij}}{\mu_{ij}}\xi\frac{\sqrt{\Delta t}}{2}. \tag{B2}$$

Similarly, Eqs. (B1c) and (B1d) may be combined to give

$$\begin{aligned}v_{ij}^e(\Delta t) &= v_{ij}^e(\Delta t/2) - d_{ij}v_{ij}^e(\Delta t)\frac{\Delta t}{2} + \frac{\sigma\omega_{ij}}{\mu_{ij}}\xi\frac{\sqrt{\Delta t}}{2} \\ &= \frac{1}{1 + d_{ij}\Delta t/2}\left[v_{ij}^e(\Delta t/2) + \frac{\sigma\omega_{ij}}{\mu_{ij}}\xi\frac{\sqrt{\Delta t}}{2}\right].\end{aligned} \tag{B3}$$

Eliminating $v_{ij}^e(\Delta t/2)$ by means of Eq. (B2) and subtracting $v_{ij}^e(0)$ from both sides of the resulting equation, we arrive at Eq. (A9).

APPENDIX C: STEADY-STATE HEAT TRANSFER

Viscous heating is the only mechanism of energy exchange between translational and internal degrees of freedom of DPD particles. For some combinations of σ and α, characterizing the viscous heating and the heat conduction dynamics, respectively, and under certain boundary conditions, a discrepancy may arise between the temperature profiles $T_k(z)$ computed from the kinetic energy of particles, and $T_i(z)$, which is based on their internal energies.

To estimate the thermal conductivity of the system using RNEMD, we suppose that the temperature profiles at a steady state are described by the following set of equations:

$$\begin{aligned}\kappa_k\frac{d^2T_k}{d\zeta^2} + \lambda(T_i - T_k) &= -\frac{\Phi}{k_B}, \\ \kappa_i\frac{d^2T_i}{d\zeta^2} + \lambda(T_k - T_i) &= \frac{\Phi}{k_B},\end{aligned} \tag{C1}$$

where the ζ axis points in the same direction as the z axis but its origin is at the center of the sampling region. The

quantity κ_k is the thermal conductivities associated with energy exchange among DPD particles through their translational degrees of freedom. Likewise, κ_i is the thermal conductivity arising from heat conduction dynamics described by Eq. (A2). The coefficient λ may be interpreted as the heat transfer coefficient describing the energy exchange between translational and internal degrees of freedom. The source term Φ/k_B represents the rate at which heat, in the form of kinetic energy of particles, is generated per unit volume of the system. In the present context, it arises from the integration scheme of the primary dynamics.

In writing Eq. (C1), we are assuming that the heat thus generated is compensated exactly by the depletion of the internal energy of particles. This is analogous to what happens in the projection method with the internal energy rescaling. In Eq. (C1), however, the balance between generation and depletion of energy is imposed at every point in space. This is an acceptable model description of the actual process in simulations at least on average and if the steady state is maintained by a proper energy controlling measure such as EDD, the projection methods, or the use of a sufficiently small time step.

Assuming that κ_k, κ_i, λ, and Φ are constant, we can readily integrate Eq. (C1) and arrive at Eq. (39), in which

$$a := \sqrt{\lambda\left(\frac{1}{\kappa_i}+\frac{1}{\kappa_k}\right)}, \tag{C2}$$

Solving Eq. (39) for T_k and T_i, we arrive at Eq. (38).

[1] L. Verlet, Phys. Rev. **159**, 98 (1967).
[2] W. C. Swope, H. C. Andersen, P. H. Berens, and K. R. Wilson, J. Chem. Phys. **76**, 637 (1982).
[3] P. J. Hoogerbrugge and J. M. V. A. Koelman, Europhys. Lett. **19**, 155 (1992).
[4] T. Shardlow, SIAM J. Sci. Comput. **24**, 1267 (2003).
[5] S. Melchionna, J. Chem. Phys. **127**, 044108 (2007).
[6] B. Leimkuhler, C. Matthews, and G. Stoltz, IMA J. Numer. Anal. **36**, 13 (2016).
[7] H. Yoshida, Phys. Lett. A **150**, 262 (1990).
[8] S. Toxvaerd, Phys. Rev. E **50**, 2271 (1994).
[9] J. Gans and D. Shalloway, Phys. Rev. E **61**, 4587 (2000).
[10] M. E. Tuckerman, *Statistical Mechanics: Theory and Molecular Simulation* (Oxford University Press, Oxford, UK, 2010).
[11] M. Lísal, J. K. Brennan, and J. B. Avalos, J. Chem. Phys. **135**, 204105 (2011).
[12] A.-A. Homman, J.-B. Maillet, J. Roussel, and G. Stoltz, J. Chem. Phys. **144**, 024112 (2016).
[13] J. B. Avalos and A. D. Mackie, Europhys. Lett. **40**, 141 (1997).
[14] P. Español, Europhys. Lett. **40**, 631 (1997).
[15] F. Müller-Plathe and P. Bordat, in *Novel Methods in Soft Matter Simulation*, Lecture Notes in Physics Vol. 640, edited by M. Karttunen, I. Vattulainen, and A. Lukkarinen (Springer, Berlin, 2004), pp. 310–326.
[16] P. Wirnsberger, D. Frenkel, and C. Dellago, J. Chem. Phys. **143**, 124104 (2015).
[17] F. A. Furtado, C. R. A. Abreu, and F. W. Tavares, AIChE J. **61**, 2881 (2015).
[18] C. Kane, J. E. Marsden, and M. Ortiz, J. Math. Phys. **40**, 3353 (1999).
[19] C. Salueña and J. B. Avalos, Phys. Rev. E **89**, 053314 (2014).
[20] B. Pace, F. Diele, and C. Marangi, Math. Comput. Simulat. **110**, 40 (2015).
[21] R. D. Engle, R. D. Skeel, and M. Drees, J. Comput. Phys. **206**, 432 (2005).
[22] D. Cottrell and P. F. Tupper, BIT Numer. Math. **47**, 507 (2007).
[23] C. P. Lowe, Europhys. Lett. **47**, 145 (1999).
[24] P. Nikunen, M. Karttunen, and I. Vattulainen, Comput. Phys. Commun. **153**, 407 (2003).
[25] E. A. J. F. Peters, Europhys. Lett. **66**, 311 (2004).
[26] B. Leimkuhler and X. Shang, J. Comput. Phys. **280**, 72 (2015).
[27] B. Leimkuhler and X. Shang, J. Comput. Phys. **324**, 174 (2016).
[28] T. Yamada, S. Itoh, Y. Morinishi, and S. Tamano, J. Chem. Phys. **148**, 224101 (2018).
[29] L. D. Landau and E. M. Lifshitz, *Statistical Physics Part 1*, 3rd ed. (Pergamon Press, New York, 1980).
[30] M. Toda, R. Kubo, and N. Saito, *Statistical Physics I: Equilibrium Statistical Mechanics*, 2nd ed. (Springer-Verlag, Berlin, 1992).
[31] I. Kusaka, *Statistical Mechanics for Engineers* (Springer, Berlin, 2015).
[32] E. A. Koopman and C. P. Lowe, J. Chem. Phys. **124**, 204103 (2006).
[33] T. Mikosch, *Elementary Stochastic Calculus: With Finance in View* (World Scientific, Singapore, 1998).
[34] M. Ripoll, P. Español, and M. H. Ernst, Int. J. Mod. Phys. C **9**, 1329 (1998).
[35] W. H. Press, S. A. Teukolsky, W. T. Vetterling, and B. P. Flannery, *Numerical Recipes* (Cambridge University Press, Cambridge, UK, 1992).
[36] See Supplemental Material at http://link.aps.org/supplemental/10.1103/PhysRevE.101.042120 for a more complete set of results.
[37] Ohio Supercomputer Center, http://osc.edu/ark:/19495/f5s1ph73.
[38] M. Serrano, G. De Fabritiis, P. Español, and P. V. Coveney, Math. Comp. Simulation **72**, 190 (2006).
[39] G. De Fabritiis, M. Serrano, P. Español, and P. V. Coveney, Phys. A (Amsterdam, Neth.) **361**, 429 (2006).